TEXTURE ANALYSIS FOR A SPD PROCESSED Ti-10Zr-5Nb-5Ta ALLOY

Vasile Dănuț COJOCARU[1], Doina RĂDUCANU[2], Ion CINCA[3], Andreea CĂPRĂRESCU[4]

Texture of Severe Plastic Deformation (SPD) processed Ti-10Zr-5Nb-5Ta alloy was investigated by X-ray diffraction. Developed texture modes observed after SPD processing were: high orientation density family modes, such as: {$01\bar{1}1$}<$10\bar{1}0$>; {$01\bar{1}2$}<$10\bar{1}0$> and {$01\bar{1}0$}<0001>; all created by deformation slip towards the end of deformation process and low to medium orientation density family mods, such as: {$11\bar{2}0$}<0001> and {$11\bar{2}6$}<$24\bar{6}\bar{1}$>; all created by twinning deformation, in early stages of deformation process.

Keywords: α titanium alloys; texture; pole figure

1. Introduction

Titanium and its alloys are widely used in aerospace, electronics, biomedical and energy applications due to their low density–strength ratio, high biocompatibility and high corrosion resistance. In all these fields, the crystallographic texture developed during thermomechanical treatments plays a crucial role on the physical properties of the material [1–3]. For this reason, texture changes in titanium alloys during cold work, primary recrystallization, grain growth and the α ↔ β phase transformation are of interest [4–7]. At ambient temperatures the microstructure of α-type Titanium alloys, may consist of an equiaxed (hexagonal close-packed, hcp) primary-alpha phase (α-Ti), which may also containing middle-like secondary-alpha (α”-Ti) phase. In special cases also the (body-centred cubic, bcc) beta phase (β-Ti) may appear due to the stress induced phase transition.

Much attention has recently been given to the influence of large plastic deformation on microstructure evolution and the resulting properties of metals and

[1] Lecturer, PostDoc fellow, National Institute for Research and Development in Microtechnologies, Romania, e-mail: dan.cojocaru@mdef.pub.ro, Materials Science and Engineering Faculty, POLITEHNICA University of Bucharest, Romania

[2] Prof., Materials Science and Engineering Faculty, POLITEHNICA University of Bucharest, Romania

[3] Prof., Materials Science and Engineering Faculty, POLITEHNICA University of Bucharest, Romania

[4] PhD student, Materials Science and Engineering Faculty, POLITEHNICA University of Bucharest, Romania

alloys. This interest arises from the substantial refinement of microstructure during heavy cold working that leads to a considerable increase in strength and fatigue life and a decrease in superplastic-forming temperature [8,9]. Typically, severe plastic deformation (SPD) has to be performed over many passes in order to achieve a homogeneous microstructure composed of ultrafine grains, so the productivity is relatively low. It is therefore difficult to scale this approach up into mass production for grain refinement. It has been demonstrated by Kim et al. [10,11] that high-ratio differential speed rolling (HRDSR) is a quite effective method of creating ultrafine-grained (UFG) microstructure in metallic alloys.

The properties of many crystalline materials depend on the individual properties of the single crystals and also on parameters characterizing the polycrystalline state. Since preferred orientations of the grains are very common phenomena, crystalline texture sometimes plays an important role in terms of numerous mechanical and physical behaviours. The texture may undergo evolution during casting, processing, deformation, welding, as well as heat treatment. There are many typical texture components simultaneously present in polycrystalline materials, so that the texture distribution is of concern. By now, the pole figures or inverse pole figures are most frequently used to characterize the texture in polycrystalline materials by using X-ray diffraction, although there are some limitations due to the two-dimensional information for three-dimensional crystallographic spaces. Orientation distribution function (ODF) is another tool that is much more precise in terms of the presentation for individual texture components.

Texture in hexagonal structural materials have attracted significant interest over the years because of the use of zirconium alloys for cladding of nuclear reactor fuels [12,13], titanium alloys for structural materials in aerospace and aircraft industry [14-17], as well as structural materials in transportation vehicles or light-weight enclosures for computer, communication and consumer electronic products [18,19].

The aim of this research is to investigate the developed α-Ti texture in the Severe Plastic Deformation (SPD) processed Ti-10Zr-5Nb-5Ta alloy (a Titanium alloy containing: α-Ti; α”-Ti and β-Ti phases), to identify the main texture modes and developed texture fibres.

2. Methods

2.1. Alloy synthesis

The investigated alloy has been produced using a vacuum induction melting in levitation furnace FIVES CELLES with nominal power 25 kW and melting capacity 30 cm^3, starting from elemental components. Resulted chemical composition in wt.% was: 75%Ti;10%Zr; 5%Nb; 5%Ta.

2.2. Severe Plastic Deformation (SPD) of the Ti-25Ta-25Nb alloy

The as-cast alloy was processed by Severe Plastic Deformation (SPD) procedure, as shown in figure 1. The SPD procedure consists in a first cold-rolling with 69.55% total deformation degree ($\varepsilon_{CR\ I\ tot}$), in 22 rolling passes. The first cold-rolling was followed by a recrystallization heat treatment at 850°C for 30 minutes, in argon protective atmosphere. The recrystallization heat treatment was performed in order to remove the effects of strain-hardening. For the recrystallization heat treatment a GERO SR 100x500 heat treatment oven was used.

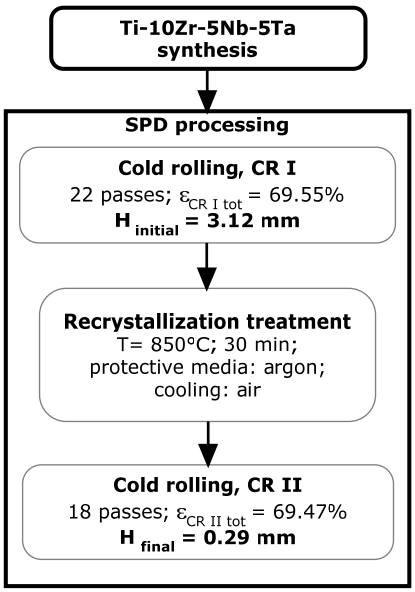

Fig. 1. SPD processing route.

After recrystallization, a second cold-rolling deformation was performed, up to 69.47% total deformation degree ($\varepsilon_{CR\ II\ tot}$), in order to obtain the final sheet thickness of about 290 μm (0.29 mm). All cold-rollings were performed using a Mario di Maio LQR120AS rolling-mill. The rolling speed was 3 m/min.

2.3. XRD experiments

SPD processed specimens were XRD characterized using a Panalytical X'Pert PRO MRD diffractometer, with a wavelength of Cu k-alpha (λ = 1.5418 A). In order to analyse the resulted texture the $(10\bar{1}1)$ pole figure was measured. The pole figure raw data was fitted and analysed, using MTEX v3.2.2 open source software package [20,21], in order to calculate de Inverse Pole Figure (IPF) and Orientation Distribution Function (ODF).

3. Results and discussion

The as-cast and SPD processed Ti-10Zr-5Nb-5Ta alloy show the presence of α-Ti, α”-Ti and β-Ti phases, as observed in Fig. 2. In the case of as-cast state the alloy contain only α-Ti and α”-Ti phases (see Fig. 2.a) while in the case of SPD state the alloy contain also the β-Ti phase (see Fig. 2.b).

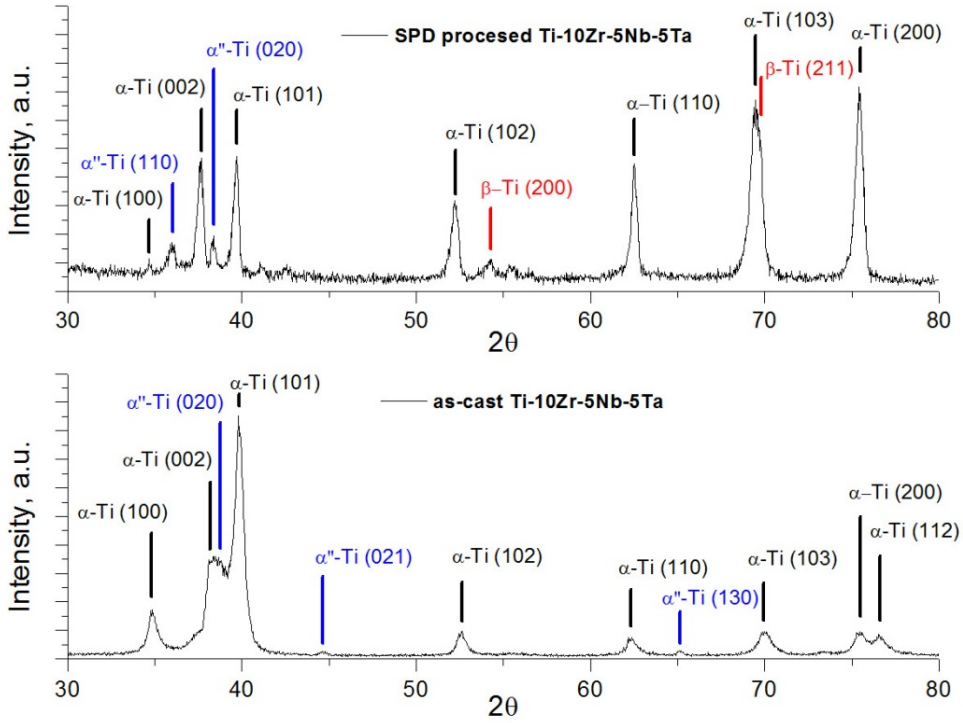

Fig. 2. XRD spectra for as-cast (a) and SPD processed (b) Ti-10Zr-5Nb-5Ta alloy

Analysing the data for as-cast state it was found that the α-Ti phase (indexed in hexagonal close-packet system - P63/mmc) has the following lattice parameters: a = 2.876 A; c = 4.608 A (a/c = 1.602). In the case of α”-Ti phase (indexed in orthorhombic system - Cmcm) the lattice parameters were as follows: a = 3.135 A; b = 4.811; c = 4.635. The α-Ti and α”-Ti phase quantities were founded to be: 95.77±0.56% and respectively 4.23±0.41%.

After SPD processing, it was found that the β-Ti phase appear due to the stress induced transformation. In this case it was found that the β-Ti phase (indexed in body centred cubic system - Im3m) has the lattice parameter a = 3.302 A. The phase quantities resulted, after SPD processing, were as follows: α-Ti - 85.87±0.51%, α”-Ti - 6.82±0.21% and respectively β-Ti - 7.31±0.74%.

The texture in rolled sheet cubic metals is represented by $\{h\ k\ l\}<u\ v\ w>$ pairs, in which the $\{h\ k\ l\}$ represents planes which lie parallel to the sheet plane, whereas $<u\ v\ w>$ direction point parallel to the rolling direction. The texture in rolled sheet hexagonal metals, are commonly represented by $\{h\ k\ i\ l\}<u\ v\ t\ w>$, which means that the $\{h\ k\ i\ l\}$ planes of these grains lie parallel to the sheet plane, whereas their $<u\ v\ t\ w>$ direction point parallel to the rolling direction. The correspondence between the 3-digit Miller indices and 4-digit Miller-Bravais indices is given by the following relation:

$$\begin{cases} i = -(h+k) \\ t = -(u+v) \end{cases} \tag{1}$$

When the texture is less complex, it is possible to describe the texture by means of a series of pole figures constructed by simple X-ray diffraction methods. However, the information contained in pole figures is incomplete and at best semi-quantitative. In fact, it is frequently not sufficient to fully determine the true and complete textures if the crystallites possess more than one preferred (ideal) orientation. The more complete orientation distribution function is unfortunately, however, not directly measured by simple X-ray diffraction, and need further derivations and calculations based on a number of experimentally measured pole figures.

Fig. 3 shows collected raw data for $(10\bar{1}1)$ pole figure. The $(10\bar{1}1)$ pole figure was plotted in respect to the following directions (sample reference frame): $[10\bar{1}0]$ – rolling direction (RD); $[01\bar{1}0]$ – transversal direction (TD) and $[0001]$ – normal direction (ND).

The $(10\bar{1}1)$ pole figure, see Fig. 3, shows intensities distributions characteristic for hcp (hexagonal close-packet) crystalline structures.

A well-developed rolling-texture is confirmed in as-rolled specimen as shown in Figs. 3. The $(10\bar{1}1)$ pole figure shows two peaks symmetrically located around 30° from the centre along RD direction. This means that the rolling direction is parallel to $[11\bar{2}0]$ crystal directions.

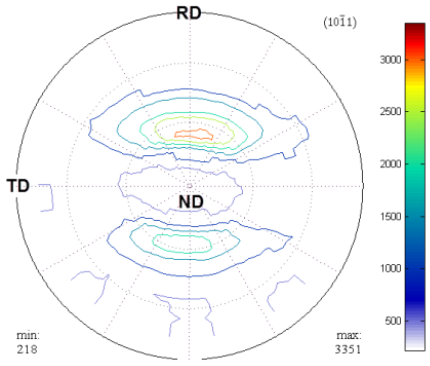

Fig. 3. 2D representation of raw data $(10\bar{1}1)$ pole figure for SPD processed Ti-10Zr-5Nb-5Ta alloy

While the pole figure shows how the specified crystallographic direction of grains are distributed in the sample reference frame, the inverse pole figure shows how the selected direction in the sample reference frame is distributed in the reference frame of the crystal. Fig. 4 shows the $(10\bar{1}1)$ inverse pole figure for RD, TD and ND directions.

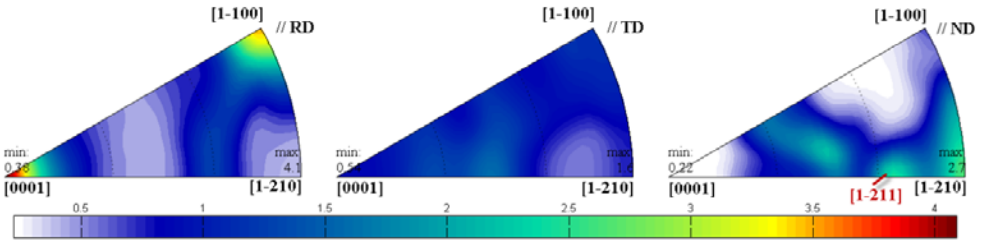

Fig. 4. Representation of $(10\bar{1}1)$ Inverse Pole Figure; a – for RD direction; b – TD direction; c – ND direction

For example, if we consider the RD direction, the inverse pole figure show us which crystallographic directions in the polycrystalline material are most likely parallel to the sample rolling direction (see Fig. 4.a), in this case one can see that the [0001]//RD pair reaches an intensity close to 4 and the $[1\bar{1}00]$//RD pair reaches an intensity close to 3.2. In the case of TD direction, can be seen that no pairs parallel to TD are formed (see Fig. 4.b). In the case of ND direction one can observe low intensity $[1\bar{2}10]$//ND and $[1\bar{2}11]$//ND pairs (see Fig. 4.c) both close to 2.5. In this way most likely the developed texture during Severe Plastic Deformation (SPD) processing will show [0001]//RD, $[1\bar{1}00]$//RD, $[1\bar{2}10]$//ND and $[1\bar{2}11]$//ND components.

Using raw pole figure data the Orientation Distribution Function was calculated and plotted. In order to calculate the ODF, few assumptions were

made: the crystalline symmetry was indexed in hexagonal 6/mmm system and the specimen symmetry in orthorhombic 222 system.

The most relevant texture mods (components) for hcp metals are [14]:

- {0001} basal fibre: including major components {0001}<10$\bar{1}$0> and {0001}<11$\bar{2}$0>;
- {10$\bar{1}$0} fibre: including major components {10$\bar{1}$0}<0001> and {10$\bar{1}$0}<11$\bar{2}$0>;
- {11$\bar{2}$0} fibre: including major components {11$\bar{2}$0}<0001> and {11$\bar{2}$0}<10$\bar{1}$0>;
- texture component {$\bar{1}$2$\bar{1}$4}<10$\bar{1}$0>;
- texture component {$\bar{1}$2$\bar{1}$2}<10$\bar{1}$0>;
- texture component {$\bar{1}$2$\bar{1}$1}<10$\bar{1}$0>;
- texture component {$\bar{1}$2$\bar{1}$0}<10$\bar{1}$0>.

In Fig. 5 the calculated ODF is presented in respect to reduced Euler space using the Roe system (ψ - θ - φ). The rotation angle (φ) used to section the ODF's was 60°, divided in 4 sections (15° steps).

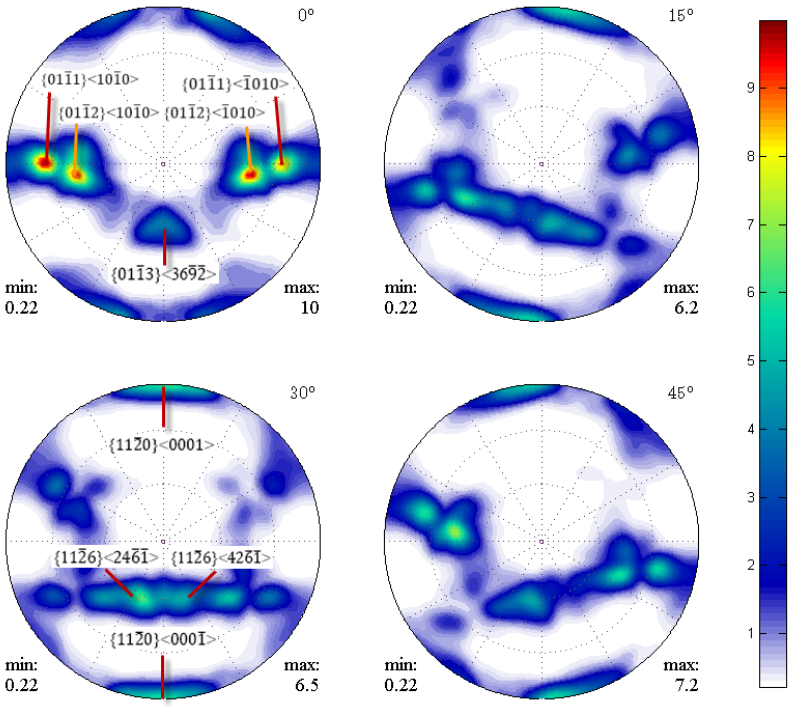

Fig. 5. Calculated Orientation Distribution Function (ODF) using Roe system for SPD processed Ti-10Zr-5Nb-5Ta alloy

In the case of hcp materials the developed texture is well characterized in $\varphi = 0°$ and $\varphi = 30°$ sections [14].

If one pays a closer look to ODF's presented in Fig. 5, can observe that for rotation angle $\varphi = 0°$ the developed texture components shows maximum intensities close to 9.7 for $\{01\bar{1}1\}<10\bar{1}0>$ and $\{01\bar{1}1\}<\bar{1}010>$ texture components (belonging to $\{10\bar{1}1\}$ fibre). A second texture mod is developed in $\{01\bar{1}2\}<10\bar{1}0>$ and $\{01\bar{1}2\}<\bar{1}010>$ systems (belonging to $\{01\bar{1}2\}$ fibre), reaching an intensity close to 8.2. Beside the two high intensity modes a third low intensity texture mod is observed in $\{01\bar{1}3\}<36\bar{9}\bar{2}>$ system.

For rotation angle $\varphi = 30°$ the developed texture shows only medium intensity components, such as: $\{11\bar{2}0\}$ fibre (including $\{11\bar{2}0\}<0001>$ and $\{11\bar{2}0\}<000\bar{1}>$ components) and $\{11\bar{2}6\}$ fibre (including $\{11\bar{2}6\}<24\bar{6}\bar{1}>$ and $\{11\bar{2}6\}<42\bar{6}\bar{1}>$ components); all showing an intensity close to 5.5.

The crystallographic textures are typically presented, also, in the reduced Euler space using the Bunge system (φ_1 - Φ - φ_2). In Fig. 6 one can observe the calculated sections of ODF for rotation angle (φ_2) in 15° steps. Also in the Bunge representation the texture is well characterized in $\varphi_2 = 0°$ and $\varphi_2 = 30°$ sections.

In the case of $\varphi_2 = 0°$ ODF section, one can observe that the following texture mods are present:

- high intensity $\{01\bar{1}1\}$ fibre, which spreads from $\{01\bar{1}1\}<10\bar{1}0>$ to $\{01\bar{1}1\}<\bar{1}010>$; showing an orientation density close to 9.8;
- high intensity $\{01\bar{1}2\}$ fibre, which spreads from $\{01\bar{1}2\}<10\bar{1}0>$ to $\{01\bar{1}2\}<\bar{1}010>$; showing an orientation density close to 7.1;
- medium intensity $\{01\bar{1}0\}$ fibre, which spreads from $\{01\bar{1}0\}<0001>$ to $\{01\bar{1}0\}<000\bar{1}>$; with an orientation density close to 6.2;
- low intensity $\{01\bar{1}3\}<36\bar{9}\bar{2}>$ texture mod; with and orientation density close to 4.5.

Analysing the $\varphi_2 = 30°$ ODF section, one can observe that fewer texture modes are present, both low intensity with an orientation density close to 5:

- $\{11\bar{2}0\}$ fibre, which spreads from $\{11\bar{2}0\}<0001>$ to $\{11\bar{2}0\}<000\bar{1}>$;
- $\{11\bar{2}6\}$ fibre, which spreads from $\{11\bar{2}6\}<24\bar{6}\bar{1}>$ to $\{11\bar{2}6\}<42\bar{6}\bar{1}>$.

Calculated texture characteristics for developed texture during SPD processing shows a maximum orientation distribution for $\{01\bar{1}1\}<\bar{1}010>$ fiber, and the textured volume in $\{01\bar{1}1\}<\bar{1}010>$ texture mod of about 17.26% (see Table 1).

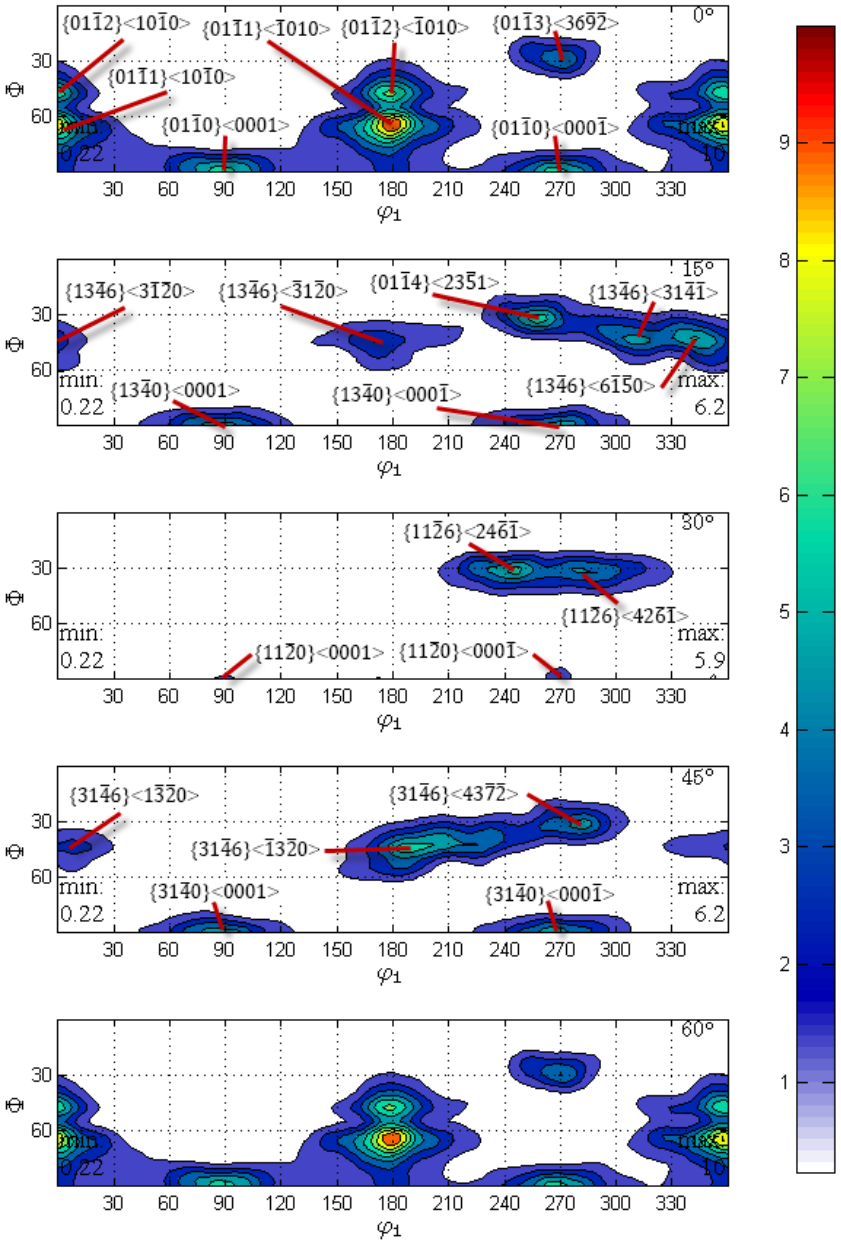

Fig. 6. Sections of the Orientation Distribution Function (ODF) for SPD processed Ti-10Zr-5Nb-5Ta alloy using Bunge system; a – $\varphi_2 = 0°$; b – $\varphi_2 = 15°$; c – $\varphi_2 = 30°$; d – $\varphi_2 = 45°$; e – $\varphi_2 = 60°$

If we take into account that $\{01\bar{1}1\}$ fiber spreads from $\{01\bar{1}1\}<10\bar{1}0>$ to $\{01\bar{1}1\}<\bar{1}010>$ and both mods shows approximately same orientation density, results that the SPD processing produce a $\{01\bar{1}1\}$ fiber volume close to 34.5 %.

Table 1

Maximum modal orientation for SPD processed Ti-10Zr-5Nb-5Ta alloy

Texture modal orientation (MO)	φ_1 [°]	179.44
	Φ [°]	64.21
	φ_2 [°]	0.455
	Texture component $\{h\ k\ i\ l\}<u\ v\ t\ w>$	$\{01\bar{1}1\}<\bar{1}010>$
Texture volume with same MO [%]		17.26
Texture index		2.392

During the plastic deformation of the alloy, grain orientation changes take place as a consequence of shear on specific favourable oriented crystal planes and directions by slip and twinning. Hexagonal polycrystals may lack the required five independent slip systems for the accommodation of an arbitrary plastic deformation. Even when five independent slip systems are available, the difference between the critical resolved shear stresses of the different crystallographic families is quite important which leads to an important plastic anisotropy at the single crystal level. Thus, the main problem of hexagonal metals is the limited ductility and the poor room temperature formability which are primarily due to the restricted number of slip systems [22]. However, at high temperatures and moderate strain rates, hexagonal metals can be ductile and readily formable. The basal and the prismatic <*a*> slip systems are mutually orthogonal and thus possess only four independent slip systems. Usually, pyramidal <*c*+*a*> slip systems are much harder to activate [23-25]. Therefore, hcp metals are often nearly inextensible along their c-axis. In addition to crystallographic slip, hcp polycrystals exhibit a greater tendency to mechanical twinning than cubic materials [22]. In hexagonal materials the slip system can exist in the following slip systems $\{h\ k\ i\ l\}<u\ v\ t\ w>$ where $\{h\ k\ i\ l\}$ is the slip plane and $<u\ v\ t\ w>$ is the slip direction) [22, 23]:

- basal slip: $\{0001\}<2\bar{1}\bar{1}0>$;
- prismatic slip: $\{01\bar{1}0\}<2\bar{1}\bar{1}0>$; $\{01\bar{1}0\}<\bar{2}113>$; $\{01\bar{1}0\}<0001>$;
- pyramidal slip: $\{10\bar{1}1\}<\bar{1}2\bar{1}0>$; $\{10\bar{1}1\}<\bar{2}113>$; $\{11\bar{2}1\}<\bar{2}113>$; $\{2\bar{1}\bar{1}2\}<\bar{2}113>$.
-

Twinning usually provides additional deformation and may relax the requirement for five independent slip systems. However, twinning is a polar mechanism (only allowing simple shear in one direction, rather than both forward and backward directions) and furthermore, the amount of strain that twinning can

accommodate is proportional to the volume fraction of crystals which have twinned. Twinning depends strongly on temperature, alloying content, stacking fault energy and crystal lattice structure [26]. Most common twinning systems in α-Ti alloys are [27, 28]:

- $\{10\bar{1}2\}<10\bar{1}\bar{1}>$; $\{10\bar{1}1\}<10\bar{1}\bar{2}>$;
- $\{11\bar{2}2\}<11\bar{2}\bar{3}>$; $\{11\bar{2}1\}<\bar{1}\bar{1}26>$.

Analysing the observed texture modes, mainly high orientation density family modes (orientation density > 5), such as: $\{01\bar{1}1\}<10\bar{1}0>$; $\{01\bar{1}2\}<10\bar{1}0>$ and $\{01\bar{1}0\}<0001>$ we can observe that all texture mods are created due to deformation slip, by prismatic <*a*> and pyramidal <*a*+*c*> slip. For low and medium orientation density family modes (orientation density < 5), such as: $\{11\bar{2}0\}<0001>$ and $\{11\bar{2}6\}<24\bar{6}\bar{1}>$ we can observe that both family modes were created by twinning deformation, in early stages of deformation process. A similar behaviour was reported also in CP-titanium [22].

In the case of α-Ti alloys it was reported [29,30] that at low-to-medium levels of levels of thickness reduction (deformation < 40%) resulted in the development of heterogeneous microstructures due to the fragmentation of some grains as a result of twinning and the elongation of other grains that deformed by slip alone.

The formation of deformation twins during cold rolling contributed to the significant refinement in microstructure and hence reduced the effective slip length. Formation of numerous mechanical twins and intersection among these twins divide the grain interior, resulting in microstructural refinement. Additional grain refinement occurred by the almost simultaneous formation of secondary and the tertiary twins in addition to subdivision of twins due to crossing twins. Twinning became saturated at 40% thickness reduction [29, 30]. At thicknesses reduction above 40% the effective grain size had been reduced to such a large extent that twinning is impossible [29, 30]. These grains deformed mainly by dislocation slip and, as a result, became elongated grains, which were comparatively larger than those that underwent twinning.

4. Conclusions

The microstructure of SPD processed Ti-10Zr-5Nb-5Ta alloy is characterized by the presence of:

- α-Ti, α”-Ti and β-Ti phases; both α”-Ti and β-Ti phases being produced by stress induced transformations;
- high orientation density family mods (orientation density > 5), such as: $\{01\bar{1}1\}<10\bar{1}0>$; $\{01\bar{1}2\}<10\bar{1}0>$ and $\{01\bar{1}0\}<0001>$; all created by deformation slip towards the end of deformation process (for thickness reduction > 40 %);

- low to medium orientation density family mods (orientation density < 5), such as: $\{11\bar{2}0\}<0001>$ and $\{11\bar{2}6\}<24\bar{6}\bar{1}>$; both family mods were created by twinning deformation, in early stages of deformation process (for thickness reduction < 40 %).

Acknowledgement

This paper was supported by the project "Human Resource Development by Postdoctoral Research on Micro and Nanotechnologies", Contract POSDRU/89/1.5 /S/63700, project co-funded from European Social Fund through Sectorial Operational Program Human Resources 2007-2013.

R E F E R E N C E S

[1] *I. Lonardelli, N. Gey, H.R. Wenk, M. Humbert, S.C. Vogel and L. Lutterotti*, "In situ observation of texture evolution during α → β and α → β phase transformations in titanium alloys investigated by neutron diffraction" in Acta Materialia, **vol. 55**, 2007, pp. 5718–5727

[2] *M.L. Weaver and H.Garmestani*, "Microstructures and mechanical properties of commercial titanium foils processed via the melt overflow process" in Materials Science and Engineering A**,** vol. 247, 1998, **pp.** 229-238.

[3] *M.R. Bache and W.J. Evans*, "Impact of texture on mechanical properties in an advanced titanium alloy" in Materials Science and Engineering A**,** vol. 319, 2001, **pp.** 409-414.

[4] *A.N. Kalinyuk, N.P. Trigub, V.N. Zamkov, O.M. Ivasishin, P.E. Markovsky, R.V. Teliovich and S.L. Semiatin*, "Microstructure, texture, and mechanical properties of electron-beam melted Ti–6Al–4V" in Materials Science and Engineering A**,** vol. 346, 2003, **pp.** 178-188.

[5] *S. Zaefferer*, "A study of active deformation systems in titanium alloys: dependence on alloy composition and correlation with deformation texture" in Materials Science and Engineering A**,** vol. 344, 2003, **pp.** 20-30.

[6] *S.L. Semiatin, P.N. Fagin, M.G. Glavicic, I.M. Sukonnik and O.M. Ivasishin*, "Influence on texture on beta grain growth during continuous annealing of Ti–6Al–4V" in Materials Science and Engineering A**,** vol. 299, 2001, **pp.** 225-234.

[7] *L. Zeng and T.R. Bieler*, "Effects of working, heat treatment, and aging on microstructural evolution and crystallographic texture of α, α′, α″ and β phases in Ti–6Al–4V wire" in Materials Science and Engineering A**,** vol. 392**,** 2005**, pp.** 403-414.

[8] *S.V. Zherebtsov, G.S. Dyakonov, A.A. Salem, S.P. Malysheva, G.A. Salishchev and S.L. Semiatin*, "Evolution of grain and subgrain structure during cold rolling of commercial-purity titanium" in Materials Science and Engineering A, **vol. 528**, 2011, pp. 3474-3479.

[9] *X.D. Wang, H.B. Lou, K. Stahl, J. Bednarcik, H. Franz and J.Z. Jiang*, "Tensile behavior of orthorhombic α''-titanium alloy studied by in situ X-ray diffraction" in Materials Science and Engineering A, **vol. 527**, 2010, pp. 6596-6600.

[10] *W.J. Kim, K.E. Lee and S.H. Choi*, "Mechanical properties and microstructure of ultra fine-grained copper prepared by a high-speed-ratio differential speed rolling" in Materials Science and Engineering A**,** vol. 506**,** 2009**, pp.** 71-79.
[11] *W.J. Kim, M.J. Kim and J.Y. Wang*, "Ultrafine-grained Mg–9Li–1Zn alloy sheets exhibiting low temperature superplasticity" in Materials Science and Engineering A**,** vol. 516**,** 2009**, pp.** 17-22.
[12] *G.C. Kaschner and G.T. Gray*, "The influence of crystallographic texture and interstitial impurities on the mechanical behavior of zirconium" in Metallurgical and Materials Transactions A, **vol. 31**, 2000, pp. 1997-2003.
[13] *J.J. Fundenberger, M.J. Philippe, F. Wanger and C. Esling*, "Modelling and prediction of mechanical properties for materials with hexagonal symmetry (zinc, titanium and zirconium alloys)" in Acta Materialia**,** vol. 45**,** 1997**, pp.** 4041-4055.
[14] *Y.N. Wang and J.C. Huang*, "Texture analysis in hexagonal materials" in Materials Chemistry and Physics, **vol. 81**, 2003, pp. 11-26.
[15] *N. Gey and M. Humbert*, ""Characterization of the variant selection occurring during the α→β→α phase transformations of a cold rolled titanium sheet in Acta Materialia**,** vol. 50**,** 2002**, pp.** 277-287.
[16] *S.L. Semiatin and T.R. Bieler*, "Effect of texture and slip mode on the anisotropy of plastic flow and flow softening during hot working of Ti-6Al-4V" in Metallurgical and Materials Transactions A, **vol. 32**, 2001, pp. 1787-1799.
[17] *F. Wanger, N. Bozzolo, O. Van Landutyt and T. Grosdidier*, "Evolution of recrystallisation texture and microstructure in low alloyed titanium sheets" in Acta Materialia**,** vol. 50**,** 2002**, pp.** 1245-1259.
[18] *T. Mukai, M. Yamanoi, H. Watanabe and K. Higashi*, "Ductility enhancement in AZ31 magnesium alloy by controlling its grain structure" in Scripta Materialia**,** vol. 45**,** 2001**, pp.**89-94.
[19] *S.F. Su, J.C. Huang, H.K. Lin and N.J. Ho*, "Electron-beam welding behavior in Mg-Al-based alloys" in Metallurgical and Materials Transactions A, **vol. 33**, 2002, pp.1461-1473.
[20] *F. Bachmann, R. Hielscher and H. Schaeben*, "Texture Analysis with MTEX - Free and Open Source Software Toolbox", in Solid State Phenomena, **vol. 160**, 2010, pp. 63-68.
[21] *F. Bachmann, R. Hielscher, P. E. Jupp, W. Pantleon, H. Schaeben and E. Wegert*, "Inferential statistics of electron backscatter diffraction data from within individual crystalline grains", in Journal of Applied Crystalography, **vol. 43**, 2010, pp. 1338-1355.
[22] *Y.B. Chun, S.H. Yu, S.L. Semiatin and S.K. Hwang*, "Effect of deformation twinning on microstructure and texture evolution during cold rolling of CP-titanium" in Materials Science and Engineering A, **vol. 398**, 2005, pp. 209-219.
[23] *G.W. Groves and A. Kelly*, "Independent slip systems in crystals" in Philosophical Magazine, **vol. 8**, 1963, pp. 877-887.
[24] *W.J. McG. Tegart*, "Independent slip systems and ductility of hexagonal polycrystals" in Philosophical Magazine, **vol. 9**, 1964, pp. 339-341.
[25] *Y.B. Chun, S.K. Hwang, M.H. Kim, S.I. Kwun and S.W. Chae*, "Effect of Mo addition on the crystal texture and deformation twin formation in Zr-based alloys" in Journal of Nuclear Materials, **vol. 295**, 2001, pp. 31-41.
[26] *P. Klimanek and R. Kuzel Jr*, "X-ray diffraction line broadening due to dislocations in non-cubic materials. I. General considerations and the case of elastic isotropy applied to hexagonal crystals" in Journal of Applied Crystallography, **vol. 21**, 1988, pp. 59-66
[27] *M.H. Yoo*, Slip, "Twinning, and fracture in hexagonal close-packed metals" in Metallurgical and Materials Transactions A, **vol. 12**, 1981, pp. 409-418.

[28] *M. H. Yoo, J. R. Morris, K. M. Ho and S. R. Agnew*, "Nonbasal deformation modes of HCP metals and alloys: Role of dislocation source and mobility" in Metallurgical and Materials Transactions A, **vol. 22**, 2002, pp. 813-822.

[29] *M.J. Philippe, M. Serghat, P. Van Houtte and C. Esling*, "Modelling of texture evolution for materials of hexagonal symmetry - II. application to zirconium and titanium α or near α alloys" in Acta Metallurgica et Materialia, **vol. 43**, 1995, pp. 1619-1630.

[30] *S. Mullins and B.M. Patchett*, "Deformation microstructures in titanium sheet metal" in Metallurgical and Materials Transactions A, **vol. 12**, 1981, pp. 853-863.